http://dx.doi.org/10.5935/0103-5053.20150123

J. Braz. Chem. Soc., Vol. 26, No. 8, 1551-1564, 2015.
Printed in Brazil - ©2015 Sociedade Brasileira de Química
0103 - 5053 $6.00+0.00

Article

Selective Hydrogenolysis of Glycerol to 1,2-Propanediol Over Bimetallic Cu-Ni Catalysts Supported on γ-Al_2O_3

Satyanarayana M. Pudi,[a] Prakash Biswas,[,a] Shashi Kumar[a] and Biswajit Sarkar[b]*

[a]*Department of Chemical Engineering, Indian Institute of Technology Roorkee, 247667 Roorkee, Uttarakhand, India*

[b]*Department of Chemical Engineering, University at Buffalo, The State University of New York (SUNY), 14260-4200 Buffalo-NY, USA*

A series of Cu or Ni monometallic and Cu-Ni bimetallic catalysts supported on γ-Al_2O_3 were synthesized by incipient wetness impregnation method. X-ray diffraction results exhibited the formation of bimetallic Cu-Ni phase in the reduced Cu-Ni(1:1)/γ-Al_2O_3 catalyst. Among the catalyst examined for hydrogenolysis of glycerol, bimetallic catalysts exhibited higher catalytic activity than monometallic catalysts due to synergetic effect of Cu-Ni bimetal. Cu-Ni(1:1)/γ-Al_2O_3 catalyst displayed a maximum glycerol conversion of 71.6% with 92.8% selectivity to 1,2-propanediol at 210 °C and 4.5 MPa hydrogen pressure. The superior performance of Cu-Ni(1:1)/γ-Al_2O_3 catalyst was attributed to the formation of bimetallic Cu-Ni phase, high active metal surface area, small Cu-Ni particle size, and high acidic strength of the catalyst. Stability and reusability of Cu-Ni(1:1)/γ-Al_2O_3 catalyst was performed and detailed characterization results of fresh and used catalysts suggested that bimetallic Cu-Ni phase remained stable after reuses.

Keywords: glycerol hydrogenolysis, Cu-Ni bimetallic catalysts, 1,2-propanediol, catalyst stability

Introduction

Recently, biodiesel has received considerable attention due to scarcity of fossil fuel reserves and global warming problems. Worldwide production of biodiesel is estimated to reach 1.2 billion tons by 2016, with an annual growth rate of nearly 42%.[1,2] The Indian national biofuel policy proposed a target of 20% biofuel blending (both bio-ethanol and biodiesel) with conventional fuels by 2017.[3] Glycerol is produced in surplus amounts (10 wt.%) as by-product in the production of biodiesel via transesterification of vegetable oils and fats.[4] Transformation of glycerol into value-added products is essential to improve the economic viability of biodiesel industry and biofuel supply chain. Crude glycerol can be utilized as a feed stock for the production of green chemicals. In recent years, various glycerol conversion process such as hydrogenolysis to propanediols, selective oxidation to dihydroxyacetone, etherification to fuel oxygenates, reforming to syn-gas and fermentation to 1,3-propanediol (1,3-PDO), etc. have been attempted.[4] Among these processes, selective hydrogenolysis of glycerol to 1,2-propanediol (1,2-PDO) and 1,3-PDO is an attractive and innovative pathway.[5] 1,2-PDO is a major commodity chemical used as raw material for unsaturated polyster resins, food additives, functional fluids (antifreeze, de-icing and heat transfer), paints, animal feed, cosmetics and pharmaceuticals.[6-8] Other promising chemicals such as 1,3-PDO, ethylene glycol (EG), hydroxyacetone (acetol), 1-propanol (1-PO), 2-propanol (2-PO) produced by hydrogenolysis of glycerol also have significant industrial importance.

Various noble metal (Pt, Ru, Pd, Rh, Ir and Re) and non-noble metal (Cu, Ni, Zn, Al, Fe, Mg, Si and Co) catalysts have been attempted for this reaction. Noble metal catalysts propagate the cleavage of both C–C and C–O bonds of glycerol leading to formation of degradation products.[9-16] Copper based catalysts such as Cu/Al_2O_3,[6,9,17,18] Cu-Cr,[8,19] Cu/ZnO,[13] Cu-Zn-Cr-Zr,[20] Cu containing bimetallic catalysts,[21] Cu/SiO_2,[1,22-24] Cu/MgO[25] and Cu/layered double oxides[26,27] exhibited superior performance in terms of high selectivity to 1,2-PDO, which was attributed to higher efficiency for C–O breaking in the presence of hydrogen.[20] Even though Cu-based catalysts exhibits high selectivity toward 1,2-PDO, their activity and stability requires to be

*e-mail: prakashbiswas@gmail.com; prakbfch@iitr.ernet.in

improved. Nickel based catalysts have also been studied for this reaction. Ni/NaX,[28] Ni/γ-Al_2O_3,[29,30] and Ni-Ce/SBA-15[31] catalysts have been reported as active at 150-220 °C and 1-9 MPa hydrogen pressure. Advantages associated with the use of Ni catalysts remain in their ability to promote hydrogenation-dehydrogenation reaction, which is required for obtaining important intermediate products such as acetol. However, in comparison to noble metals, Ni-based catalysts has disadvantage due to their low stability because of carbon deposition that blocks the active sites and catalyst pores.[32]

Cu-Ru on various supports,[16] Cu-X (X = Ag,Zn,Cr),[21] bimetallic catalysts for hydrogenolysis of glycerol have been reported. They suggested that bimetallic catalysts improve the catalytic activity and product selectivity due to their synergetic and bifunctional effects. Recently, Cu-Ni bimetallic catalysts have been established as effective catalysts for industrially important reactions such as steam reforming of ethanol,[33] water-gas shift reaction,[34] decomposition of methane,[35] pyrolysis of oils,[36] and hydrogenation of organic functional groups.[37] Gandarias *et al.*[38,39] studied glycerol hydrogenolysis over Cu-Ni/Al_2O_3 catalysts with 2-propanol and formic acid as hydrogen donor molecules. Maximum glycerol conversion of 70.5% with 70% selectivity to 1,2-PDO has been reported at 4.5 MPa H_2 pressure. Significant selectivity (30%) to degradation products indicated C–C bond cleavage over the Cu and Ni sites of the reduced catalysts. Selective conversion of glycerol into propanediols requires a suitable catalyst with bi-functional acid sites/metal surface, favouring the cleavage of the glycerol C–O bonds (dehydration/hydrogenation) by hydrogen and eliminating C–C bond scission.[9]

Further development of catalysts which can provide higher glycerol conversion and propanediol selectivity are necessary to ensure successful development of industrial process for hydrogenolysis of glycerol. It is important to design highly stable, active and selective catalyst to perform the reaction at low hydrogen pressure and temperature. It requires catalysts both for dehydration and hydrogenation functionality. Therefore, development of catalysts having dual active site may be a good alternative.

In this work, we have synthesized Cu, Ni monometallic and Cu-Ni bimetallic catalysts supported on γ-Al_2O_3 and investigated their performance for selective conversion of glycerol to 1,2-PDO. The effect of the Cu/Ni weight ratio on the physicochemical characteristics of the catalysts as well as the performance is evaluated. In addition, the role of bimetallic Cu-Ni formation and its bifunctional behavior for hydrogenolysis reaction has been demonstrated. Furthermore, effect of various reaction parameters such as reaction temperature, reaction pressure, reaction time, glycerol concentration, and metal loading are investigated to maximize the glycerol conversion and 1,2-PDO selectivity. Finally, the stability/reusability of the catalysts was investigated and the result obtained is discussed in support of characterization results of fresh and used catalysts.

Experimental

Materials

$Cu(NO_3)_2.3H_2O$ (> 99%, Himedia Chemicals, India), $Ni(NO_3)_2.6H_2O$ (> 99%, Merck Specialities, India) were used as metal precursors and γ-Al_2O_3 (> 99.5%, Merck specialities, India) was used as catalyst support. The standard chemicals such as glycerol (> 99%, Merck Specialities, India), 1,2-PDO (> 99%, Merck Specialities, India), 1,3-PDO (98%, Sigma Aldrich, Germany) and acetol (95%, Alfa Aesar) were used as feed and product calibration, respectively. The ultra high pure hydrogen (99.99%) and nitrogen (99.99%) were supplied by Sigma gases, India and used directly without any further purification.

Catalyst preparation

A series of Cu, Ni monometallic and bimetallic catalysts supported on γ-Al_2O_3 with a nominal metal loading of 20 wt.% were synthesized by conventional wetness impregnation method. Three different weight ratios of Cu to Ni viz. 3, 1 and 0.33 were selected for the synthesis of bimetallic catalysts. A calculated amount of metal precursors $Cu(NO_3)_2.3H_2O$ and $Ni(NO_3)_2.6H_2O$ were dissolved in Millipore water. γ-Al_2O_3 support was added to this metal precursor solution under stirring. The slurry obtained was aged for 24 h at room temperature and then dried in an oven for 12 h at 110 °C, and subsequently calcined at 400 °C in the air for 4 h.

Catalyst characterization

N_2 adsorption-desorption isotherms measurements were performed at −196 °C using a Micromeritics Accelerated Surface Area and Porosimetry (ASAP-2020) system. Prior to the analysis, samples were degassed at 300 °C for 6 h under vacuum. The surface area of all the samples were analysed employing the multipoint BET method by using adsorption data at the relative pressure (P/P_o) range of 0.05-0.3. Pore size distributions were determined by using the BJH-Halsey-Fass correction method considering the desorption branch.

CO chemisorption experiments of the catalyst samples were conducted at 40 °C using a Micromeritics ASAP 2020

instrument. Prior to the chemisorption analysis, the catalyst samples were degassed under vacuum for 5 h at 250 °C to remove chemisorbed gases and moisture present, if any. Catalyst samples of approximately 250 mg were evacuated at 120 °C under the flow of helium for 45 min before being reduced at 350 °C in a hydrogen flow for 90 min. After cooling the sample under vacuum to 40 °C, the adsorption isotherms were recorded.

X-ray diffraction (XRD) patterns were recorded with a Bruker AXS D8 Advance diffractometer equipped with Cu-Kα radiation source (λ = 0.154 nm). All the data were recorded at the 2θ interval of 10-80° with a steep of 0.02° s^{-1} and a time constant of 3s.

Temperature programmed reduction (TPR) was performed to determine the reduction behavior of catalysts. The experiments were performed on the Micromeritics Pulse Chemsorb 2720 equipment. Typically, 25 mg of catalyst sample was dried at 120 °C overnight in an oven prior to TPR experiment. The dried catalyst sample was placed in a U-shaped quartz reactor and further pre-treated at 150 °C for 2 h under the nitrogen flow (30 cc min^{-1}), followed by cooling at room temperature. After pre-treatment, the temperature was raised from room temperature to 850 °C at a rate of 10 °C min^{-1} in a 10% H_2/Ar flow (20 cc min^{-1}). A thermal conductivity detector (TCD) was employed to determine the amount of hydrogen consumed.

NH_3-temperature programmed desorption (NH_3-TPD) was carried out on a Micromeritics Pulse Chemsorb 2720 instrument equipped with TCD. Typically, 80 mg of reduced catalyst sample was dried at 120 °C overnight in an oven prior to TPD experiment. The catalyst sample was further degassed under stream of helium (20 cc min^{-1}) at 150 °C for 2 h then cooled to room temperature. Further, sample was saturated with NH_3 by flowing 27% NH_3/He gas mixture (30 cc min^{-1}) for 1 h. After being purged helium for 1 h to remove the physically absorbed ammonia, the sample was heated from 30 to 800 °C at a heating rate of 15 °C min^{-1} and the NH_3 desorption was monitored with a TCD.

Total Cu and Ni metal contents in fresh and used catalysts were determined by inductive coupled plasma-mass spectrometer (ICP-MS). Approximately 20 mg of catalyst and 2 mL of aqua regia (0.5 mL of nitric acid and 1.5 mL of hydrochloric acid) were placed in a 15 mL glass vial fitted with a teflon lined cap digested in an oven at 140 °C for 30 min. Then the samples were prepared by dilution with Millipore water to required concentrations (< 1 ppm). Perkin-Elmer Elan DRC-e ICP-MS was used for the elemental detection.

To explore the morphology and composition of the catalysts, scanning electron microscopy (SEM) images were collected using Quanta scanning electron microscope (Model 200 FEG, USA) equipped with energy dispersive X-ray spectra (EDX). Catalyst sample was dispersed uniformly on the sample holders and coated with gold using sputter coater (Edwards S150) and then SEM images were taken at an acceleration voltage of 20 kV under vacuum.

The particle sizes of the fresh and spent catalysts were recorded by transmission electron microscope (TEM) (Tecnai G^2 20 S-Twin, FEI Netherlands). The samples were dispersed by a sonicator in ethanol before placing them on carbon coated copper grid.

Catalytic reaction

Hydrogenolysis of glycerol was carried out in a 250 mL teflon lined stainless steel autoclave reactor (Model No. 2000, Amar equipments) equipped with an electronic temperature controller, a mechanical stirrer and a liquid sampling port. Prior to each test, the catalyst was reduced in a separate tubular reactor unit in a stream of pure hydrogen (50 cc min^{-1}) for 3 h at a temperature corresponding to the reduction temperature obtained from the TPR study of each catalyst. Initially, the autoclave reactor was fed with 100 mL of aqueous glycerol (20 wt.%) along with calculated amount of catalyst and then purged with hydrogen for three times. The reactor temperature was set at 210 °C and pressurized the reactor vessel with hydrogen up to 4.5 MPa. The stirring speed was set constant at 700 rpm and the product sample was collected after 12 h of reaction for analysis. The stability of the catalyst was explored in repeated experiments in order to test their reusability.

The reactant and products were analysed by gas chromatograph (GC 6800, Newchrom Technologies) equipped with flame ionization detector (FID) and a Chromosorb-101 packed column (1.52 m × 3.1 mm OD × 2 mm ID). The liquid products were centrifuged (Heraeus Biofuge Stratos, Thermo Scientific) to separate any catalyst particles present prior to GC analysis. For calculating the selectivity of the products, *n*-butanol was used as an internal standard. The results reported in this study are reproduced by repeating the experiments three times and carbon balance was 100 ± 3.5%.

The glycerol conversion, product selectivity and yield are defined as follows:

$$\text{Conversion}\,(\%) = \frac{\text{Moles of glycerol converted}}{\text{Total moles of glycerol in feed}} \times 100 \quad (1)$$

$$\text{Selectivity}\,(\%) = \frac{\text{Moles of carbon in speci c product}}{\text{Total carbon moles in all liquid products}} \times 100 \quad (2)$$

$$\text{Yield}\,(\%) = \frac{\text{Conversion}\,(\%) \times \text{Selectivity}\,(\%)}{100} \quad (3)$$

Results and Discussion

Catalyst characterization

Nitrogen adsorption-desorption isotherms of Cu-Ni/γ-Al_2O_3 catalysts with different copper to nickel metal weight ratios are shown in Figure 1. Typical type-IV isotherms with a pronounced hysteresis loop type H2 with a steep incline at a relative pressure of $0.50 < P/P_o < 0.90$ are observed. This result represents a typical mesoporous nature of catalysts.[40,41]

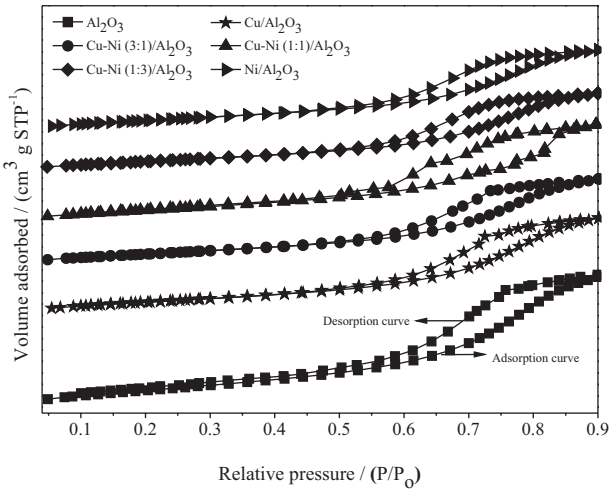

Figure 1. Nitrogen adsorption-desorption isotherms of Cu/γ-Al_2O_3, Ni/γ-Al_2O_3 and Cu-Ni/γ-Al_2O_3 catalysts.

For all the catalysts, textural properties such as BET surface area (S_{BET}), cumulative pore volume (V_p) and average pore diameter (D_p) data obtained is shown in Table 1. The surface area of γ-Al_2O_3 is 107 m^2 g^{-1}, whereas for metal doped catalysts, surface area values are in the range of 67-78 m^2 g^{-1}. The surface areas of the catalysts decrease nearly about 25-35% after metal impregnation. The reduction of surface area in mesoporous supported catalysts is more pronounced as reported earlier.[23] Pore volume of all the catalysts is found to be in the range of 0.12-0.15 cm^3 g^{-1}, which is lower than γ-Al_2O_3 (0.20 cm^3 g^{-1}). Pore volume of catalysts is decreased due to the structural collapse of precursors during calcination of the catalyst after metal impregnation.[42] Measured pore diameter of all catalysts is in the range of 55-59 Å.

The metal dispersion values of the catalysts obtained from CO chemisorption follow the order: Ni/γ-Al_2O_3 > Cu-Ni/γ-Al_2O_3 > Cu/γ-Al_2O_3 suggests that the size of Cu is higher than Cu-Ni and Ni size (Table 1). Therefore, the bigger Cu particles could block the pores of the Al_2O_3 structure and reduce the surface accessible for adsorption.[38] The metallic surface area (S_m) of the catalysts obtained from CO chemisorption analysis is in the range of 2.5-10.8 m^2 g^{-1} sample (Table 1).

The XRD patterns were recorded in order to identify the crystalline phase and crystal structure of catalysts. Figure 2 shows XRD patterns of calcined Cu/γ-Al_2O_3, Ni/γ-Al_2O_3 and Cu-Ni/γ-Al_2O_3 catalysts, respectively.

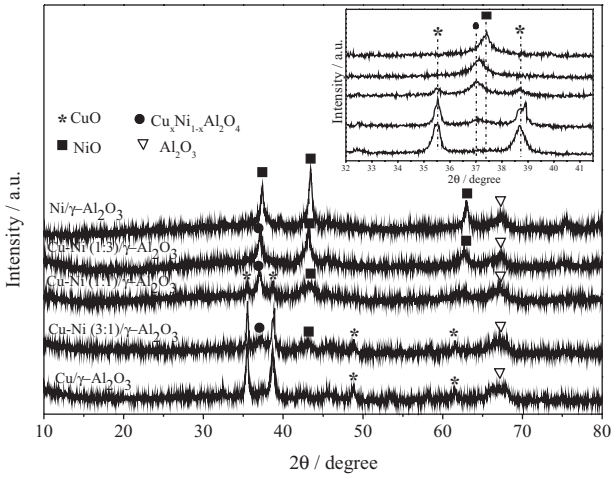

Figure 2. XRD patterns of calcined Cu/γ-Al_2O_3, Ni/γ-Al_2O_3 and Cu-Ni/γ-Al_2O_3 catalysts with 20 wt.% metal loading at different Cu/Ni metal ratio. Diffraction patterns in the angles between 32° and 42° (inset).

XRD pattern of Cu/γ-Al_2O_3 catalyst shows the diffraction peaks at 2θ = 35.5°, 38.7°, 48.6° and 61.5°,

Table 1. Textural properties of catalysts and support

Catalyst	Metal loading[a] / wt.%		S_{BET}[b] / (m^2 g^{-1})	V_p[b] / (cm^3 g^{-1})	D_p[b] / Å	CO_{irr} uptake / (μmol g^{-1})	Metal dispersion,[c] D / %	Metallic surface area,[c] S_m / (m^2 g^{-1} sample)
	Cu	Ni						
γ-Al_2O_3	–	–	107	0.20	57	–	–	–
Cu/γ-Al_2O_3	19.8	–	77	0.15	59	62.0	1.9	2.5
Cu-Ni(3:1)/γ-Al_2O_3	14.2	8.3	67	0.13	57	96.0	2.5	3.3
Cu-Ni(1:1)/γ-Al_2O_3	7.4	11.7	78	0.15	56	112.0	3.3	4.3
Cu-Ni(1:3)/γ-Al_2O_3	5.4	16.3	69	0.12	55	97.7	2.6	3.5
Ni/γ-Al_2O_3	–	16.8	71	0.12	55	348.0	8.1	10.8

[a]Data obtained from SEM-EDX results; [b]data obtained from BET adsorption-desorption isotherms; [c]data obtained from CO chemisorption analysis.

respectively, corresponding to (111), (111), (202) and (113) crystal planes of monoclinic CuO (JCPDS: 41-0254). The broad peak observed at 2θ = 67.5° for all catalysts is corresponding to Al_2O_3 (JCPDS: 86-1410). Peak intensities detected for Cu/γ-Al_2O_3 catalysts indicate that CuO is very well crystalline in nature. In case of Cu-Ni/γ-Al_2O_3 bimetallic catalysts, additional peaks are detected at 2θ = 43.2° and 63°, which correspond to (012) and (110) planes of NiO (JCPDS: 44-1159). With the increase in nickel loading, the peak intensities for NiO increase significantly (Figure 2). For bimetallic catalysts, apart from CuO and NiO peaks, an additional peak appears at 2θ = 36.9°, which represents mixed metal oxide phase $Cu_xNi_{(1-x)}Al_2O_4$ (x = 0.25, 0.5, 0.75) (JCPDS: 78-1602, 78-1603, 78-1604) in agreement with the previous study.[43] The intensity of the peak corresponding to mixed metal oxide phase increases with increasing amount of Ni in bimetallic catalysts (inset of Figure 2). The formation of mixed oxides indicates the strong interaction of Cu, Ni with the alumina support.[39,43] XRD pattern of Ni/γ-Al_2O_3 catalyst shows sharp peaks at 2θ = 37.3°, 43.2° and 62.8° are corresponding to NiO (JCPDS: 44-1159), which reflect the typical rhombohedral structure. Peak intensities of CuO and NiO in bimetallic catalysts are of lower intense and broader than that of monometallic catalysts, which indicate better dispersion of metal oxide on the alumina support for bimetallic catalysts as compared to monometallic catalysts.[39]

Diffraction patterns of reduced Cu/γ-Al_2O_3, Ni/γ-Al_2O_3 and Cu-Ni/γ-Al_2O_3 catalysts are shown in Figure 3. For Cu/γ-Al_2O_3 and Cu-Ni(3:1)/γ-Al_2O_3 catalysts, sharp reflection of metallic Cu is observed at 2θ = 43.3°, 50.4°, and 74.2° corresponds to (111), (200) and (220) planes of the cubic pore structure (JCPDS: 85-1326). XRD patterns of Cu-Ni(1:3)/γ-Al_2O_3 and Ni/γ-Al_2O_3 catalysts show peaks at 2θ = 44.5°, 51.8°, and 76.4°, respectively, which represent (111), (200) and (220) planes of cubic Ni metal (JCPDS: 04-0850). Additional peaks of nickel oxide are observed at 2θ = 43.2° and 62.8° in case of Ni/γ-Al_2O_3 catalyst.

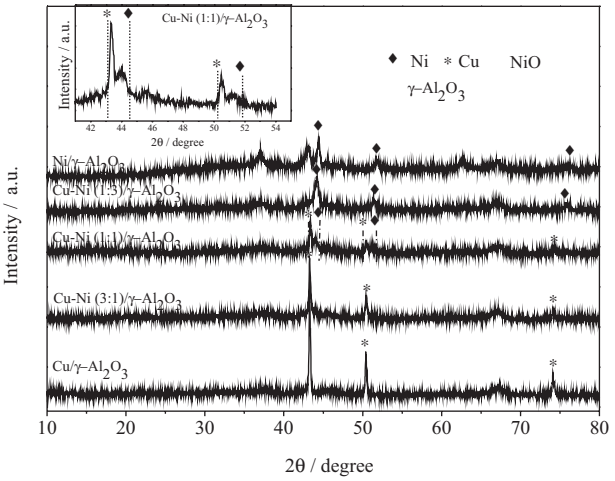

Figure 3. XRD patterns of reduced Cu/γ-Al_2O_3, Ni/γ-Al_2O_3 and Cu-Ni/γ-Al_2O_3 catalysts with 20 wt.% metal loading at different Cu/Ni metal ratio. Combined peaks for Cu-Ni bimetallic phase (inset figure).

XRD pattern of Cu-Ni(1:1)/γ-Al_2O_3 catalyst exhibits two combined diffraction peaks in between the 2θ range of 43.3°-44.5° and 50.4°-52° (inset of Figure 3), corresponding to Cu-Ni combined bimetallic phase.[34,44,45] For all the reduced catalysts, low intensity peaks for γ-Al_2O_3 are observed at 2θ = 36.8° and 67.5°, respectively. Reflection corresponding to metallic Cu is not observed in Cu-Ni(1:3)/γ-Al_2O_3 catalyst and peak corresponding to metallic Ni is not detected in Cu-Ni(3:1)/γ-Al_2O_3 is may be due to the presence of lower metal content of respective metal or complete dispersion on the support.

The average crystallite size of CuO, NiO, $Cu_xNi_{(1-x)}Al_2O_4$ and the particle size of Cu and Ni is calculated using the Scherrer equation from the line width of their respective XRD peaks (Table 2).

For calcined catalysts, the average crystallite size of CuO is estimated from X-ray line width of the peaks corresponding to (002), (111) and (202) crystal planes, respectively. The calculated dimension of CuO crystallite is in the range of 37-64 nm. The average size of NiO crystallite is in the range of 10-31 nm calculated from line width of

Table 2. Average crystallite sizes of CuO, NiO and Cu-Ni mixed oxide and Cu, Ni average particle size calculated by Scherrer equation

Catalyst	Average crystallite size / nm			Average particle size / nm	
	Calcined			Reduced[a]	
	CuO	NiO	$Cu_xNi_{(1-x)}Al_2O_4$	Cu	Ni
Cu/γ-Al_2O_3	37	–	–	89	–
Cu-Ni(3:1)/γ-Al_2O_3	64	–	28	80	–
Cu-Ni(1:1)/γ-Al_2O_3	56	10	28	33	22
Cu-Ni(1:3)/γ-Al_2O_3	–	30	32	–	29
Ni/γ-Al_2O_3	–	31	–	–	39

[a]Catalyst reduction conditions: reduction temperature of catalysts determined by TPR analysis; H_2 flow = 50 cc min^{-1}; time = 3 h.

(111), (200) and (220) crystal planes. The crystallite size of $Cu_xNi_{(1-x)}Al_2O_4$ mixed oxide phase is estimated from line width of the peak corresponding to (311) crystal plane and it is in the range of 28-32 nm (Table 2). For the reduced catalysts except for Cu-Ni (1:1), the size of the Cu particle increases due to the particle agglomeration resulted by change of surface electronic properties of Cu particles, which indicates less metal support interaction.[22,23] In case of Cu-Ni(1:1)/γ-Al_2O_3 catalyst, the size of the Cu particle estimated from line width of the peaks corresponding to (111), (200) and (220) crystal planes is decreased from 56 to 33 nm after the reduction. The nickel particle size estimated from line width of the peaks corresponding to (111), (200) and (220) crystal planes is increased from 10 to 22 nm. However, the average crystallite size of reduced catalyst is decreased slightly from 31.3 to 27.5 nm indicates the strong metal support interaction between Cu and Ni atoms which prevent sintering.[34]

The reduction behavior of Cu-Ni catalysts is analyzed by H_2-TPR (Figure 4). The reduction profile of pure γ-Al_2O_3 is characterized by a broad small intensity peak at 670 °C, which may be due to the reduction impurity present.[46] Cu/γ-Al_2O_3 catalyst exhibits two reduction peaks at 250 °C and 344 °C, respectively. The peak at the lower temperature represents the reduction of highly dispersed CuO on γ-Al_2O_3, while the peak at higher temperature represents the reduction of bulk CuO particles.[47-50] Two step reduction of bulk CuO particles was reported earlier.[47] In the two step reduction, the first step involved for the reduction of CuO to Cu^+ at 307 °C and other peak at the 327 °C is for the reduction of the Cu^+ ion to metallic copper (Cu^0). The reduction profile obtained for Ni/γ-Al_2O_3 displays a broad multiple reduction profile at 350-580 °C with a major peak at 477 °C and two shoulder peaks at 366 °C and 431 °C, respectively. The low intensity shoulder peak

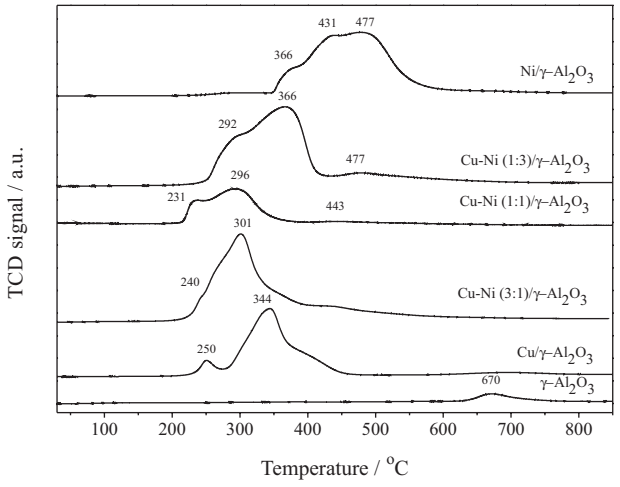

Figure 4. H_2-TPR profiles of catalysts and support.

observed at 367 °C represents the reduction of NiO to Ni^0 [51,52] and weaker shoulder peak at 431 °C is associated with the reduction of NiO having strong interaction with the support.[53] However, a broad reduction peak at 477 °C indicates the presence of bulk NiO crystallites strongly bonded with γ-Al_2O_3 support.[54] The TPR patterns of bimetallic catalysts are different from those of supported pure monometallic CuO and NiO catalysts. They exhibit combined broad peaks indicating that the reduction process for the bimetallic oxide system is more complicated than for the monometallic oxides. The reduction profiles of Cu-Ni(3:1)/γ-Al_2O_3 and Cu-Ni(1:3)/γ-Al_2O_3 catalysts display broad multiple reduction profile at 200-400 °C and 220-430 °C, respectively. Moreover, Cu-Ni(1:1)/γ-Al_2O_3 catalyst gets reduced at the temperature range of 200-340 °C. The lowest reduction temperature of 231 °C for Cu-Ni(1:1)/γ-Al_2O_3 catalyst demonstrates the strong interaction between CuO-NiO metal oxides due to the formation of bimetallic Cu-Ni. Lin *et al.*[34] reported the similar kind of TPR profiles for Cu-Ni bimetallic catalysts.

The NH_3-TPD patterns for all catalysts are shown in Figure 5. The quantitative estimation of acidic site distribution at different regions according to the desorbed amount of ammonia is summarized in Table 3. The results show that the acidic sites are distributed in three different regions, i.e., at 80-250 °C, 250-500 °C and above 500 °C for all the catalysts. It is observed from the literature that the first region is attributed to the desorption of ammonia from weak acidic sites, the second region refers to moderate strength acidic sites, and the third region represents desorption of ammonia from strong acidic sites.[55,56]

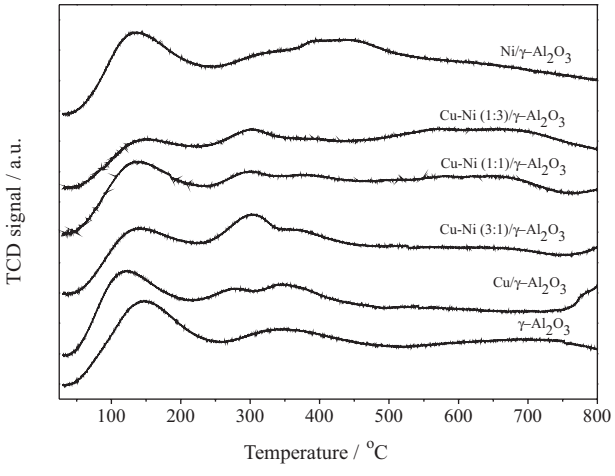

Figure 5. NH_3-TPD profiles of catalysts and support.

The NH_3-TPD profile of γ-Al_2O_3 surface displays the peaks in all three regions and shows the highest acidic strength of 1.203 mmol NH_3 $gcat.^{-1}$. The results

reported in Table 3 depict that, the acidic strength of catalysts is decreased significantly after metal impregnation. The concentration of acidic sites is decreased in the order: Cu-Ni(1:3)/γ-Al_2O_3 > Cu-Ni(3:1)/γ-Al_2O_3 > Cu-Ni(1:1)/γ-Al_2O_3 > Cu/γ-Al_2O_3 > Ni/γ-Al_2O_3. The total acidity of the bimetallic catalysts was higher due to the synergetic interaction of copper, nickel and γ-Al_2O_3 support.

Table 3. NH_3-TPD results for all catalysts

Catalyst	Acidity / (mmol NH_3 gcat.$^{-1}$)			
	Weak	Medium	Strong	Total acidity
Cu/γ-Al_2O_3	0.409	0.153	–	0.562
Cu-Ni(3:1)/γ-Al_2O_3	0.347	0.356	–	0.703
Cu-Ni(1:1)/γ-Al_2O_3	0.315	0.251	0.043	0.609
Cu-Ni(1:3)/γ-Al_2O_3	0.446	0.382	0.065	0.893
Ni/γ-Al_2O_3	0.192	0.205	0.010	0.407
γ-Al_2O_3	0.625	0.455	0.123	1.203

The crystal morphology of all the reduced catalysts is similar to *quasi*-spherical, agglomerated nanoparticles of ca. 50 nm (Figure 6a-e). Particle agglomeration is caused by sintering of particles during heat treatments.[57] EDX elemental mapping is used to determine the distribution of Cu, Ni metal on the surface of γ-Al_2O_3 and the elemental compositions obtained are summarized in Table 1. Theoretical metal loading and the metal loading obtained by EDX show an error within 5-10%. Similar kind of results were also reported earlier.[58]

Catalytic performance

Catalytic activity and product selectivity are examined over Cu, Ni monometallic and bimetallic catalysts at 210 °C and 4.5 MPa hydrogen pressure. The effect of the Cu/Ni weight ratio on catalytic activity, product selectivity and 1,2-PDO yield are determined. The catalytic results obtained are shown in Table 4.

Bimetallic catalysts exhibit glycerol conversion in the range of 45.4-59.3%, which are higher than that of monometallic catalysts (Table 4). This higher glycerol conversion for Cu-Ni bimetallic catalysts is due to the presence of bi-functionality[12,17,59] and high acidic strength (0.61-0.90 mmol NH_3 gcat.$^{-1}$).[21,27] Cu-Ni(1:1)/γ-Al_2O_3 catalyst exhibits the highest glycerol conversion of 59.3%, whereas, Cu-Ni(3:1)/γ-Al_2O_3 and Cu-Ni(1:3)/γ-Al_2O_3 catalysts display a slightly lower glycerol conversion of 46.8% and 45.4%, respectively. Higher glycerol conversion over Cu-Ni(1:1)/γ-Al_2O_3 catalyst can be attributed to synergetic effect of Cu-Ni bimetal along with high

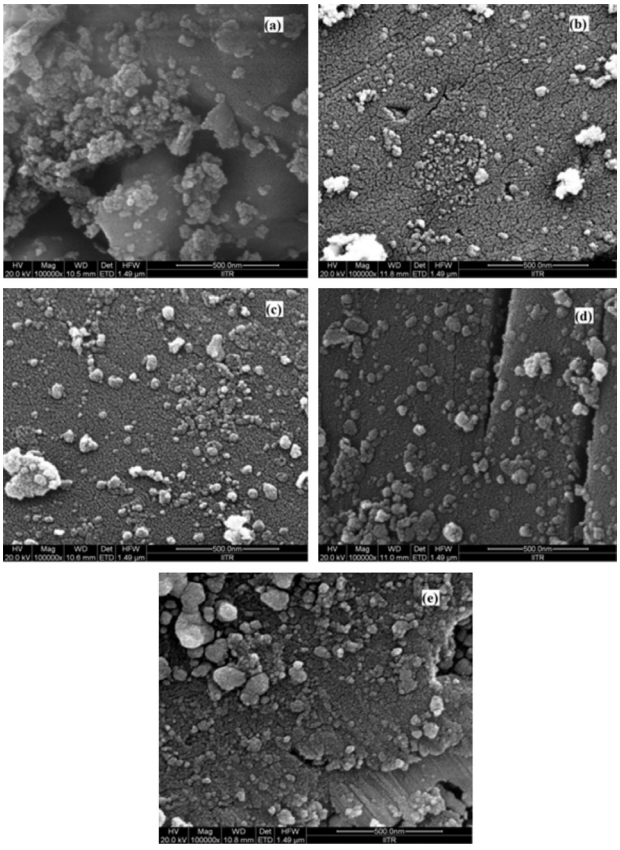

Figure 6. SEM images of (a) Cu/γ-Al_2O_3, (b) Cu-Ni(3:1)/γ-Al_2O_3, (c) Cu-Ni(1:1)/γ-Al_2O, (d) Cu-Ni(1:3)/γ-Al_2O and (e) Ni/γ-Al_2O_3 catalysts.

metallic surface area (4.3 $m^2\ g^{-1}$), small average Cu-Ni particle size (27 nm), and higher metal dispersion (3.3%). Turnover frequency (TOF) values calculated for all Cu-Ni catalysts after 12 h of reaction are shown in Table 4. TOF values are in the range of 4.7 to 53.4 h^{-1}. The highest TOF of 53.4 h^{-1} is obtained for Cu-Ni(1:1)/γ-Al_2O_3 catalyst indicates that glycerol conversion rates are correlated with TOF values. High TOF values for bimetallic catalysts due to the synergetic effect between metals in these catalysts that enhanced the overall hydrogenolysis activity. Similar TOF values were reported in literature for Ru/C,[15] Cu/layered double oxides,[27] Ru/CsPW,[59] and Ru-Cu/TiO_2 [60] catalysts. Recently, it has been reported that the activity of 20 wt.% Cu/SiO_2 catalyst increases with increasing metal surface area and TOF was higher for the catalysts with small particle size.[23] The linear dependency of the turn over number (TON) with copper metal surface area has been reported and it has been shown that the higher TON found with CuO(60)-ZnO(40) catalyst having the highest metallic surface.[24]

Cu/γ-Al_2O_3 and Ni/γ-Al_2O_3 catalysts exhibit lower glycerol conversion of 21% and 14.5%, respectively. Lower conversion of Cu/γ-Al_2O_3 catalyst can be explained by the presence of weak acidic strength (0.562 mmol NH_3 gcat.$^{-1}$)

Table 4. Catalytic behavior of Cu-Ni catalysts in glycerol hydrogenolysis

Catalyst	Conversion / %	Selectivity / %				1,2-PDO yield / %	TOF[b] / h^{-1}
		1,2-PDO	Acetol	1-Propanol	Others[a]		
Cu/γ-Al_2O_3	21.0	91.1	3.3	4.8	0.8	19.1	32.5
Cu-Ni(3:1)/γ-Al_2O_3	46.8	88.2	1.4	8.0	2.3	41.2	50.6
Cu-Ni(1:1)/γ-Al_2O_3	59.3	86.6	0.6	7.8	4.9	51.3	53.4
Cu-Ni(1:3)/γ-Al_2O_3	45.4	86.4	1.0	8.1	4.4	39.2	49.1
Ni/γ-Al_2O_3	14.5	87.9	3.0	2.8	6.1	12.7	4.7

[a]Others: ethylene glycol, 2-propanol, traces of ethanol and methanol; [b]TOF calculated by the number of moles of glycerol converted *per* moles of exposed copper atom *per* unit time (h^{-1}). Reaction conditions: glycerol concentration: 20 wt.%; reaction temperature: 210 °C; H_2 pressure: 4.5 MPa; reaction time: 12 h; catalyst wt.: 2 g; rpm: 700.

(Table 3) and larger Cu particle size (89 nm) (Table 2). For Ni/γ-Al_2O_3 catalysts, the catalytic activity is found low although the metal dispersion (8.1%) and the metallic surface area (10.8 $m^2 g^{-1}$) are higher. For Ni/γ-Al_2O_3 catalyst, the selectivity to other products (EG and methanol) is higher (6.1%), which indicates the formation of degradation products (EG and methanol) due to the breaking of C–C bond by following a different reaction path. This result explains that, Cu is more active and selective to 1,2-PDO as compared to Ni. In contrast to our results, 35 wt.% Ni/Al_2O_3 catalyst showed comparable activity to Cu-Ni bimetallic catalysts at 220 °C, 4.5 MPa N_2 pressure in the presence of formic acid as a hydrogen donor.[39] It is claimed that Ni played an active role in utilizing the hydrogen coming from formic acid. In the present study, the selectivity results suggest that, Ni promotes C–C bond cleavage, which tend to act as a source of carbon that blocks the active sites and catalyst pores. Ni/γ-Al_2O_3 catalyst is found to be least active, which may be related to lack of active sites on Ni/γ-Al_2O_3.

For all catalysts, main reaction products are 1,2-PDO, acetol and 1-propanol (Table 4). Minor amounts of other products such as ethylene glycol, 2-propanol, ethanol and methanol are also detected. All catalysts show high selectivity of 86-91% towards 1,2-PDO and combined selectivity to all remaining products including propanols, acetol, ethylene glycol, ethanol and methanol is in the range of 9-13%.

Transformation of glycerol to 1,2-PDO can proceed in two possible reaction routes. First one is a two-step process: dehydration of glycerol to acetol and hydrogenation of acetol to 1,2-PDO.[6,8,17-24,60-62] The second route is a three-step process: glycerol dehydrogenates to glyceraldehydes then dehydration to 2-hydroxyacrolein followed by hydrogenation to 1,2-PDO.[10,11,15,27] Product distribution obtained in this study suggests that the reaction proceeds through the first reaction route. A very high selectivity for 1,2-PDO (> 86%) and very low selectivity (< 3.5 %) for acetol are found after 12 h of reaction in the presence of Cu-Ni bimetallic catalysts. These selectivity values indicate a very fast hydrogenation of acetol to 1,2-PDO. Low selectivity of acetol suggests that acetol is formed by dehydration of glycerol in the presence of acidic sites of catalysts quickly hydrogenated to 1,2-PDO in presence of active metal sites.[38] Selectivity for 1-propanol and other degradation products obtained by the cleavage of C–C bond is less than 5%. This result indicates that Cu-Ni/γ-Al_2O_3 catalysts propagate selective hydrogenation of C–O bonds and limits C–C bond scission.

High glycerol conversion (59.3%) is obtained in the presence of Cu-Ni(1:1)/γ-Al_2O_3 catalyst at 210 °C and 4.5 MPa hydrogen pressure. Under this reaction condition, 1,2-PDO selectivity and yield are 86.6% and 51.3%, respectively. This suggests that, bimetallic Cu-Ni promotes C–O hydrogenolysis of glycerol and limits the selectivity of cracked products. Recently, 31% conversion of glycerol has been reported over Cu (28 wt.%)-Ni (7.7 wt.%)/Al_2O_3 catalysts at comparatively higher reaction temperature (220 °C) at this reaction condition, 84.7% selectivity and 26.2% yield for 1,2-PDO has been reported.[39] Glycerol conversion obtained in the present study is comparable with literature at relatively lower copper-nickel metal loading, lower catalyst concentration, and at relatively lower reaction temperature of 210 °C. However, 1,2-PDO selectivity (86.6%) and yield (51.3%) obtained are significantly higher than previously reported values.

Reaction parameter studies

To optimize glycerol conversion and 1,2-PDO selectivity, the effect of reaction temperature, hydrogen pressure, reaction time, glycerol concentration, catalyst amount, and metal loading on hydrogenolysis of glycerol is examined in the presence of Cu-Ni(1:1)/γ-Al_2O_3 catalyst. In the following sections, we discussed the influence of those reaction parameters on the role of Cu-Ni(1:1)/γ-Al_2O_3 catalyst in glycerol conversion and 1,2-PDO selectivity.

Effect of reaction temperature

Glycerol conversion increases from 17.5% (190 °C) to 73.2% (230 °C) (Figure 7) at 4.5 MPa H_2 pressure in the presence of Cu-Ni(1:1)/γ-Al_2O_3 catalyst.

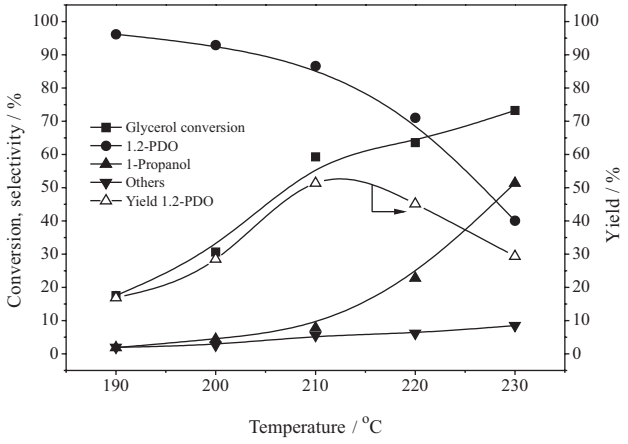

Figure 7. Effect of reaction temperature on conversion, selectivity and yield over Cu-Ni(1:1)/γ-Al_2O_3 catalyst. Others: ethylene glycol, acetol, 2-propanol, traces of ethanol and methanol. Reaction conditions: glycerol concentration: 20 wt.%; H_2 pressure: 4.5 MPa; reaction time: 12 h; catalyst wt.: 2 g; rpm: 700.

The selectivity of 1,2-PDO decreases from 96.1% at 190 °C to 40% at 230 °C and selectivity for 1-propanol and other products increases with increasing temperature. The overall yield of 1,2-PDO increased from ca. 15% at 190 °C to a maximum of 51.3% at 210 °C, and then decreased on further increase in temperature (Figure 7). TOF values are observed in the range of 15.4-64.2 h^{-1}, as the temperature increases from 190 to 230 °C. These results suggest that at higher temperature (> 210 °C), 1,2-PDO undergoes further hydrogenolysis that lead to C–C bond cleavage and produce 1-propanol and low molecular alcohols such as ethylene glycol, ethanol, and methanol.[6,8,25]

Effect of hydrogen pressure

Glycerol conversion and 1,2-PDO selectivity are increased from 34% to 62% and 69.2% to 93%, respectively, when increase in hydrogen pressure from 1.5 MPa to 6 MPa (Figure 8).

The increase in glycerol conversion with increasing pressure is due to the availability of more hydrogen species at the catalyst surface at elevated hydrogen pressures.[8,17] TOF values are found to be in the range of 32.7-53.4 h^{-1} with increasing pressure from 1.5 to 6 MPa. At higher hydrogen pressure, the concentration of active hydrogen species increases on the metal surface, which enhances the rate of hydrogenation of acetol to 1,2-PDO.[19,29] The

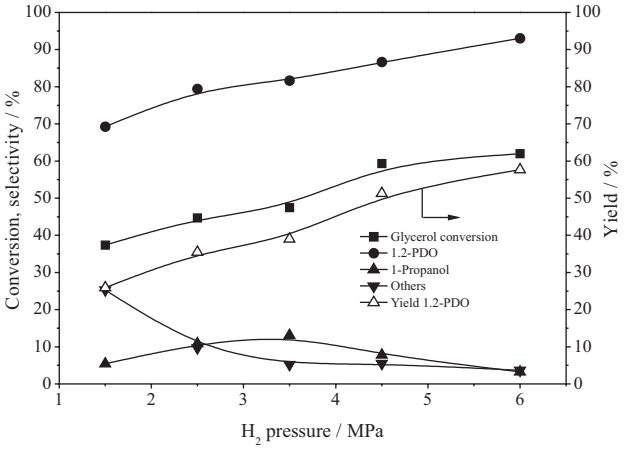

Figure 8. Effect of hydrogen pressure on conversion, selectivity and yield over Cu-Ni(1:1)/γ-Al_2O_3 catalyst. Others: ethylene glycol, acetol, 2-propanol, traces of ethanol and methanol. Reaction conditions: glycerol concentration: 20 wt.%; reaction temperature: 210 °C; reaction time: 12 h; catalyst wt.: 2 g; rpm: 700.

selectivity for 1-propanol found to be ca. 10% and the selectivity of other degradation products decreased from 25.3 to 3.6%. Overall 1,2-PDO yield increases from 25.9% at 1.5 MPa to 57.7% at 6 MPa hydrogen pressure.

Effect of reaction time

Glycerol conversion increases with increasing reaction time and reaches ca. 94% after 36 h of reaction (Figure 9).

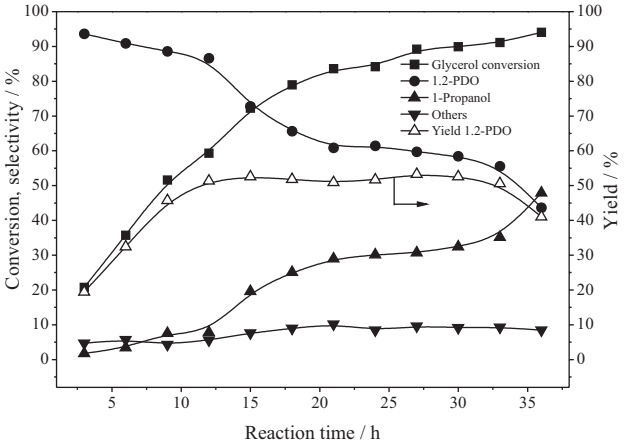

Figure 9. Effect of reaction time on conversion, selectivity and yield over Cu-Ni(1:1)/γ-Al_2O_3 catalyst. Others: ethylene glycol, 2-propanol, traces of ethanol and methanol. Reaction conditions: glycerol concentration: 20 wt.%; reaction temperature: 210 °C; H_2 pressure: 4.5 MPa; catalyst wt.: 2 g; rpm: 700.

Initially, 93.6% selectivity of 1,2-PDO is achieved after 3 h of reaction, and it decreases to 43.6% after 36 h. Simultaneously, the selectivity of 1-propanol increases from 1.7 to 47.9% and of other products increases from 4.7 to 10%, respectively. The decrease in 1,2-PDO selectivity

is due to over hydrogenolysis of 1,2-PDO which produces 1-propanol and other products.[19,23] The yield of 1,2-PDO initially increases from 19.4% to 51.3% after 12 h of reaction. Thereafter, it remains constant (ca. 52%) up to 30 h and finally it decreases to 41% after 36 h. The decrease in 1,2-PDO yield after 30 h reaction time can be attributed to the formation of by-products due to excessive C–C bond scission. The calculated TOF values are found to be in the range of 26.1-76.4 h^{-1} as the increasing time from 3 to 36 h.

Effect of glycerol concentration

The conversion of glycerol decreases with increasing glycerol concentration (Figure 10). Possible reason for the decrease in glycerol conversion is due to the availability of a limited number of active sites to convert glycerol to 1,2-PDO. The decrease in glycerol conversion with increasing glycerol concentration is consistent with the published literature.[20,25,27] TOF was calculated at different glycerol concentration and it varies in the range of 25.1-76.8 h^{-1}. Overall selectivity of 1,2-PDO decreases from 95.2% to 65.5% with increasing glycerol concentration from 10 to 80 wt.%. However, the extent of decrease in selectivity is higher at lower glycerol concentration and 1,2-PDO selectivity becomes almost constant (ca. 70%) above 30 wt.%. The decreasing trend of 1,2-PDO selectivity with increasing glycerol concentration can be attributed to formation of 1-propanol. Yield of 1,2-PDO decreased from 58.2% to 15% as glycerol concentration increases from 10 wt.% to 80 wt.%.

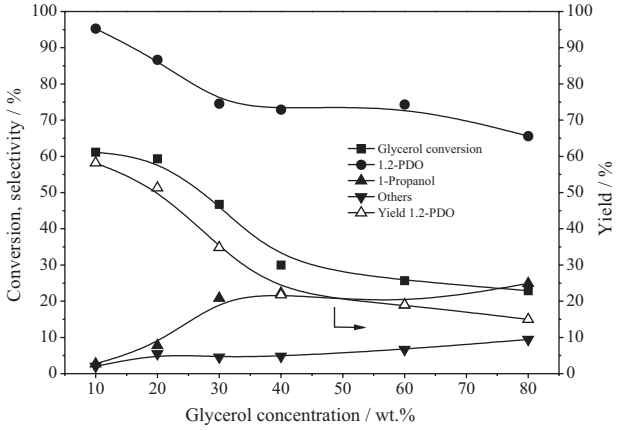

Figure 10. Effect of glycerol concentration on conversion, selectivity and yield over Cu-Ni(1:1)/γ-Al_2O_3 catalyst. Others: ethylene glycol, acetol, 2-propanol, traces of ethanol and methanol. Reaction conditions: reaction temperature: 210 °C; H_2 pressure: 4.5 MPa; reaction time: 12 h; catalyst wt.: 2 g; rpm: 700.

Effect of catalyst amount

A sharp increase in glycerol conversion (12.9-59.3%) is observed when amount of catalyst increases from 0.5 to 2 g (Figure 11). Further increase in catalyst amount (> 2 g), a gradual increase in glycerol conversion is observed. The maximum glycerol conversion of 71.5% is obtained in the presence of 4 g of catalyst in the reaction mixture. The conversion increases with increasing catalyst amount is attribute to the increase in accessibility of active catalyst surface.[8,25] The selectivity to 1,2-PDO increased from 67% to 94% when the amount of catalyst increases from 0.5 to 4 g. Overall 1,2-PDO yield increases from 8.6 to 66.4%. 1-Propanol selectivity decreases from 28.4 to 2.5% with increasing catalyst amount and the change in selectivity to other products is insignificant. As the increase in catalyst amount from 0.5 to 4 g, the TOF data is found to be in the range of 24.1-53.4 h^{-1}. This results suggest that, high active surface area favours the selective conversion of glycerol to 1,2-PDO following the dehydration-hydrogenation route eliminating the side reaction which produce the degradation products.

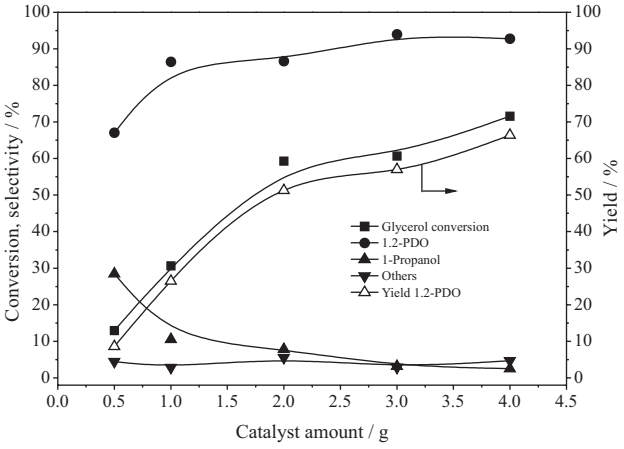

Figure 11. Effect of catalyst amount on conversion, selectivity and yield over Cu-Ni(1:1)/γ-Al_2O_3 catalyst. Others: ethylene glycol, acetol, 2-propanol, traces of ethanol and methanol. Reaction conditions: glycerol concentration: 20 wt.%; reaction temperature: 210 °C; H_2 pressure: 4.5 MPa; reaction time: 12 h; rpm: 700.

Effect of total metal loading in catalyst

As the metal loading increases from 5 to 20 wt.%, glycerol conversion increases from 32 to 59.3%, 1,2-PDO selectivity decreases slightly from 89.4 to 86.6%, and overall yield of 1,2-PDO increases from 28.6 to 51.3% (Figure 12). The increase in glycerol conversion with increasing metal loading (up to 20 wt.%) can be attributed to the increase in active metallic sites.[6,63] Further increase in metal loading up to 30 wt.%, results a marginal decrease in glycerol conversion (57.3%), which is due to the presence of larger catalyst particles. It is reported earlier that at higher metal loading (4 mmol Cu g^{-1} support), the total active meta sites decreases due to the formation of larger

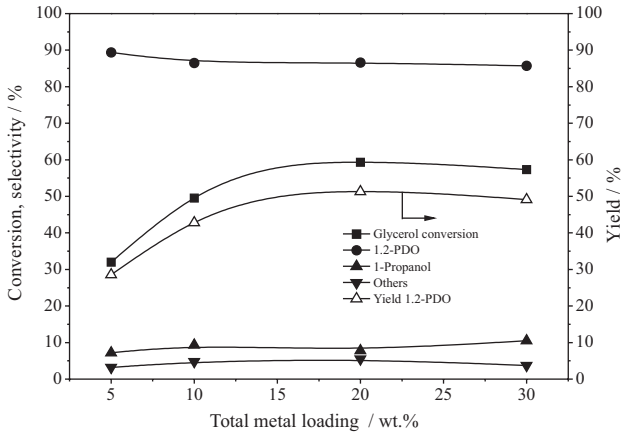

Figure 12. Effect of total metal loading on conversion, selectivity and yield over Cu-Ni(1:1)/γ-Al_2O_3 catalyst. Others: ethylene glycol, acetol, 2-propanol, traces of ethanol and methanol. Reaction conditions: glycerol concentration: 20 wt.%; reaction temperature: 210 °C; H_2 pressure: 4.5 MPa; reaction time: 12 h; catalyst wt.: 2 g; rpm: 700.

Cu crystallites in Cu/Al_2O_3 catalyst, which decreases the dispersion and facilitates the blockage of pores on the support as well.[6] 1,2-PDO selectivity (86%) and yield (50%) are almost constant above 20 wt.% metal loading. 1-Propanol selectivity increases from 5 to 10.5% and of other products remains unchanged throughout.

Reusability of catalyst

Deactivation behavior and reusability of 20 wt.% Cu-Ni(1:1)/γ-Al_2O_3 catalyst are examined at 210 °C and 4.5 MPa H_2 pressure with 20 wt.% glycerol as feed for 12 h. Prior to each cycle of experiment, the catalyst was separated by filtration and washed with deionised water followed by ethanol, and then dried overnight at 110 °C. This dried catalyst was reduced under hydrogen environment at 350 °C before further testing. Results obtained for four successive reactions are summarized in Table 5.

Glycerol conversion was moderately decreased in each cycle and it is varied from 59.3 to 44.4% in the successive cycles (Table 5). 1,2-PDO selectivity is increased from 85.6 to 93.1%, and selectivity of 1-propanol and other products are decreased from 7.8 to 3% and 5.5 to 4%, respectively. The yield of 1,2-PDO is decreased from 51.3 to 41.4%. The reason for decreased glycerol conversion is related to the loss of the catalyst during filtration and reuse process. Similar observation has also been reported in the literature for Cu-based catalysts during recycling studies.[23,27,64-66] To verify the reason of slight deactivation of the catalyst in the reuse experiments, the fresh reduced and recycle-3 catalysts were characterized by various techniques. The results obtained are discussed in the following section.

Characterization of used catalysts

Used catalyst (after cycle-3) was characterized by XRD, SEM-elemental mapping, ICP-MS and TEM methods and the results are compared with the fresh catalyst. XRD patterns of reduced, used catalysts for cycle-1 and cycle-3 are presented in Figure 13.

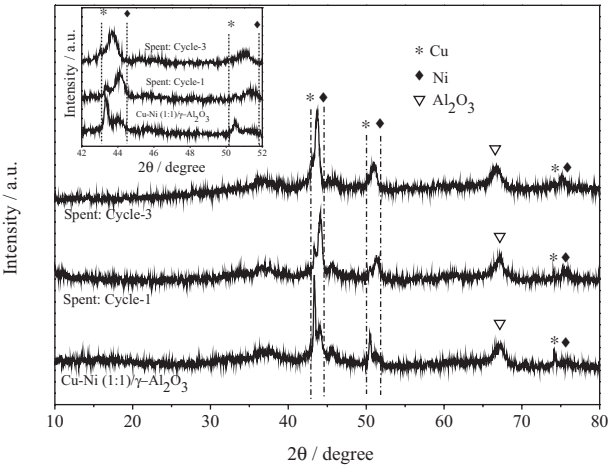

Figure 13. XRD patterns of Cu-Ni(1:1)/γ-Al_2O_3 catalyst after reaction. Combined peaks for Cu-Ni bimetallic phase (inset figure).

XRD profile of reduced catalyst shows two combined diffraction peaks of bimetallic Cu-Ni phases at the 2θ value range of 43.3-44.5° and 50.4-52°. Whereas, the XRD profiles of the spent catalyst in cycle-1 and cycle-3 exhibit mixed peaks of bimetallic Cu-Ni phase with high intensity at the same 2θ values (inset Figure 13). This result suggests

Table 5. Catalytic behavior over Cu-Ni (1:1)/γ-Al_2O_3 catalyst during recycling experiments

No. of cycles	Cu/Ni ratio Theoretical (Actual)[a]	Conversion / %	Selectivity / %			1,2-PDO yield / %
			1,2-PDO	1-Propanol	Others[b]	
Fresh reduced	1.0 (1.15)	59.3	86.6	7.8	5.5	51.3
Cycle-1	1.0 (1.21)	52.2	92.1	2.8	5.1	48.1
Cycle-2	–	47.7	92.3	3.6	4.1	44.0
Cycle-3	1.0 (1.08)	44.4	93.1	2.9	4.0	41.4

[a]Metal contents determined by ICP-MS analysis; [b]others: ethylene glycol, acetol, 2-propanol, traces of ethanol and methanol; reaction conditions: reaction temperature: 210 °C; H_2 pressure: 4.5 MPa; reaction time: 12 h; rpm: 700; catalyst/glycerol = 10 wt.%.

that the bimetallic Cu-Ni phase remain stable and strong metal-support interactions exist after prolonged contact time under hydrogen environment at 210 °C and 4.5 MPa H_2 pressure.

In order to check any possible metal loss by leaching during the reaction, the elemental composition of Cu and Ni metals in the fresh and used catalysts are determined by ICP-MS analysis. The theoretical and actual Cu/Ni ratios are presented in Table 5. The reported actual Cu and Ni metal compositions are slightly higher than the theoretical value. The Cu/Ni ratios of the spent catalysts during cycle-1 (1.21) and cycle-3 (1.08) are closer to the fresh catalyst (1.15), which confirms that the metallic properties are stable during the course of successive reactions. TEM images and selected area electron diffraction (SAED) patterns (Figure 14a-d) suggest that the morphology of used catalyst (cycle-3) remains similar to that of fresh catalyst. The SAED pattern of fresh reduced catalyst confirms the poly crystalline nature of the particles presenting diffraction planes (111), (220) associated with Cu metal (JCPDS No. 85-1326) and planes (200), (311) for metallic Ni (JCPDS No. 04-0850). The used catalyst (cycle-3) shows the diffraction planes of (111), (220) for metallic copper and (311), (331) for metallic Ni, respectively. The particle size distribution (10-60 nm) of used catalyst is similar to that of fresh reduced catalyst, which is in good agreement with XRD results (Table 2). These results suggest that particle size and dispersion of used catalysts remain the same to that of the fresh reduced Cu-Ni(1:1)/γ-Al_2O_3 catalyst even after four consecutive experiments. Thus the structural stability of the Cu-Ni(1:1)/γ-Al_2O_3 catalyst under the reaction condition remain intact. Therefore, Cu-Ni(1:1)/γ-Al_2O_3 catalyst is reusable and is promising for commercial applications.

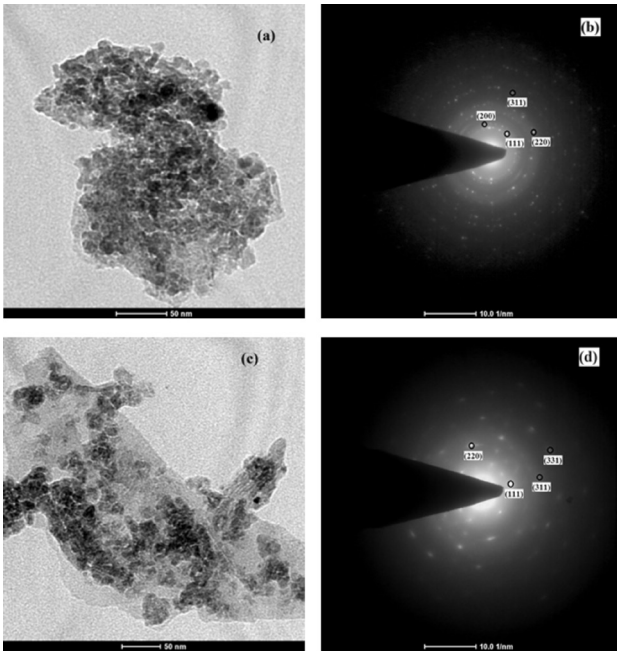

Figure 14. TEM images of 20 wt.% Cu-Ni(1:1)/γ-Al_2O_3 catalyst: (a) fresh reduced catalyst; (b) used catalyst (cycle-3) and SAED pattern of (c) fresh reduced catalyst; (d) used catalyst (cycle-3).

Conclusions

Cu/γ-Al_2O_3, Ni/γ-Al_2O_3 monometallic, and Cu-Ni/γ-Al_2O_3 bimetallic catalysts were prepared by incipient wetness impregnation method and evaluated for liquid phase hydrogenolysis of glycerol. Cu-Ni bimetallic catalysts showed higher activity (45.4-59.3%) and 1,2-PDO selectivity (86-91%) than monometallic catalysts. Cu-Ni(1:1)/γ-Al_2O_3 catalyst exhibited maximum glycerol conversion of 59.3% at 210 °C and 4.5 MPa hydrogen pressure in the presence of 2 g catalyst and after 12 h. Higher catalytic activity was ascribed to the formation of bimetallic Cu-Ni phase, high metallic surface area (4.3 $m^2 g^{-1}$), small Cu-Ni particle size (27 nm), and higher metal dispersion (3.3%). The bimetallic Cu-Ni phase favoured selective conversion of glycerol to 1,2-PDO (ca. 90% selectivity) via dehydration-hydrogenation pathway. Detailed parametric study with 20 wt.% Cu-Ni(1:1)/γ-Al_2O_3 catalyst suggested that maximum glycerol conversion of 71.6% with 93% selectivity to 1,2-PDO can be achieved at 210 °C, H_2 pressure of 4.5 MPa, glycerol concentration (20 wt.%), 12 h, and in presence of 4 g of catalyst. Reusability and structural stability of 20 wt.% Cu-Ni(1:1)/γ-Al_2O_3 catalysts were verified. ICP-MS analysis data and TEM images of fresh and used catalysts showed the catalyst morphology remain stable after successive reuses.

Acknowledgements

The authors thank DEAN, SRIC, Indian Institute of Technology Roorkee, Uttarakhand, India for supporting this work from SRIC-Fund under F.I.G. (Scheme-A). The authors are also grateful to the Department of Science and Technology (DST), Government of India for financial support under the FTYS scheme (SR/FTP/ETA-0032/2011, DATED 21.2.2012). S. N. M. P. thank MHRD for the award of fellowship.

References

1. Vasiliadou, E. S.; Eggenhuisen, T. M.; Munnik, P.; de Jongh, P. E.; de Jong, K. P.; Lemonidou, A. A.; *Appl. Catal., B* **2014**, *145*, 108.
2. Meher, L. C.; Gopinath, R.; Naik, S. N.; Dalai, A. K.; *Ind. Eng. Chem. Res.* **2009**, *48*, 1840.

3. http://www.bioenergyconsult.com/major-obstacles-in-indias-biodiesel-program/ accessed in April 2015.
4. Pagliaro, M.; Ciriminna, R.; Kimura, H.; Rossi, M.; Pina, C. D.; *Angew. Chem., Int. Ed.* **2007**, *46*, 4434.
5. Chauvel, A.; Lefebvre, G.; *Petrochemical Processes Technical and Economical Characteristics*; Editions Technip: Paris, 1989.
6. Guo, L.; Zhou, J.; Mao, J.; Guo, X.; Shuguang, Z.; *Appl. Catal., A* **2009**, *367*, 93.
7. http://www.nrel.gov/docs/fy04osti/35523.pdf accessed in April 2015.
8. Dasari, M. A.; Kiatsimkul, P. P.; Sutterlin, W. R.; Suppes, G. J.; *Appl. Catal., A* **2005**, *281*, 225.
9. Nakagawa, Y.; Tomishige, K.; *Catal. Sci. Technol.* **2011**, *1*, 179.
10. Montassier, C.; Menezo, J. C.; Hoang, L. C.; Renaud, C.; Barbier, J.; *J. Mol. Catal.* **1991**, *70*, 99.
11. Lahr, D. G.; Shanks, B. H.; *J. Catal.* **2005**, *232*, 386.
12. Balaraju, M.; Rekha, V.; Devi, B. L. A. P.; Prasad, R. B. N.; Prasad, P. S. S.; Lingaiah, N.; *Appl. Catal., A* **2009**, *354*, 82.
13. Chaminand, J.; Djakovitch, L.; Gallezot, P.; Marion, P.; Pinel, C.; Rosier, C.; *Green Chem.* **2004**, *6*, 359.
14. Miyazawa, T.; Kusunoki, Y.; Kunimori, K.; Tomishige, K.; *J. Catal.* **2006**, *240*, 213.
15. Maris, E. P.; Davis, R. J.; *J. Catal.* **2007**, *249*, 328.
16. Liu, H.; Liang, S.; Jiang, T.; Han, B.; Zhou, Y.; *Clean: Soil, Air, Water* **2010**, *12,* 1835.
17. Mane, R. B.; Hengne, A. M.; Ghalwadkar, A. A.; Vijayanand, S.; Mohite, P. H.; Pot-dar, H. S.; Rode, C. V.; *Catal. Lett.* **2010**, *135*, 141.
18. Vila, F.; Granados, M. L.; Ojeda, M.; Fierro, J. L. G.; Mariscal, R.; *Catal. Today* **2012**, *187*, 122.
19. Xiao, Z.; Li, C.; Xiu, J.; Wang, X.; Williams, C. T.; Liang, C.; *J. Mol. Catal. A: Chem.* **2012**, *365*, 24.
20. Sharma, R. V.; Kumar, P.; Dalai, A. K.; *Appl. Catal., A* **2014**, *477*, 147.
21. Zhou, J.; Guo, L.; Guo, X.; Mao, J.; Zhang, S.; *Green Chem.* **2010**, *12,* 1835.
22. Haung, Z.; Cui, F.; Xue, J.; Zuo, J.; Chen, J.; Xia, C.; *Catal. Today* **2012**, *183*, 42.
23. Vasiliadou, E. S.; Lemonidou, A. A.; *Appl. Catal., A* **2011**, *396*, 177.
24. Bienholz, A.; Hofmann, H.; Claus, P.; *Appl. Catal., A* **2011**, *391*, 153.
25. Balaraju, M.; Jagadeeswaraiah, K.; Prasad, P. S. S.; Lingaiah, N.; *Catal. Sci. Technol.* **2012**, *2*, 1967.
26. Yuan, Z.; Wang, L.; Wang, J.; Xia, S.; Chen, P.; Hou, Z.; Zheng, X.; *Appl. Catal., B* **2011**, *101*, 431.
27. Xia, S.; Nie, R.; Lu, X.; Wang, L.; Chen, P.; Hou, Z.; *J. Catal.* **2012**, *296*, 1.
28. Zhao, J.; Yu, W.; Chen, C.; Miao, H.; Ma, H.; Xu, J.; *Catal. Lett.* **2010**, *134*, 184.
29. Huang, L.; Zhu, Y.; Zheng, H.; Li, Y.; Zeng, Z.; *J. Chem. Technol. Biotechnol.* **2008**, *83*, 1670.
30. Miranda, B. C.; Chimentao, R. J.; Santos, J. B. O.; Gispert-Guirado, F.; Llorca, J.; Medina, F.; Lopez Bonillo, F.; Sueiras, J. E.; *Appl. Catal., B* **2014**, *147*, 464.
31. Jiménez-Morales, I.; Vila, F.; Mariscal, R.; Jiménez-López, A.; *Appl. Catal., B* **2012**, *117-118*, 253.
32. Chen, I.; Shiue, D. W.; *Ind. Eng. Chem. Res.* **1988**, *27*, 429.
33. Vizcaino, A. J.; Carrero, A.; Calles, J. A.; *Int. J. Hydrogen Energy* **2007**, *32*, 1450.
34. Lin, J. H.; Biswas, P.; Guliants, V. V.; Misture, S.; *Appl. Catal., A* **2010**, *387*, 87.
35. Reshetenko, T. V.; Avdeeva, L. B.; Ismagilov, Z. R.; Chuvilin, A. L.; Ushakov, V. A.; *Appl. Catal., A* **2003**, *247*, 51.
36. Ardiyanti, A. R.; Khromova, S. A.; Venderbosch, R. H.; Yakovlev, V. A.; Heeres, H. J.; *Appl. Catal., B* **2012**, *117-118*, 105.
37. Shi, T.; Li, H.; Yao, L.; Ji, W.; Au, C. T.; *Appl. Catal., A* **2012**, *425-426*, 68.
38. Gandarias, I.; Arias, P. L.; Requies, J.; El Doukkali, M.; Güemez, M. B.; *J. Catal.* **2011**, *282*, 237.
39. Gandarias, I.; Requies, J.; Arias, P. L.; Armbruster, U.; Martin, A.; *J. Catal.* **2012**, *290*, 79.
40. Liu, F.; Kong, W.; Qi, C.; Zhu, L.; Xiao, F. S.; *ACS Catal.* **2012**, *2*, 565.
41. Batista, A. H. M.; Ramos, F. S. O.; Braga, T. P.; Lima, C. L.; de Sousa, F. F.; Barros, E. B. D.; Filho, J. M.; de Oliveira, A. S.; de Sousa, J. R.; Valentini, A.; Oliveira, A. C.; *Appl. Catal., A* **2010**, *382*, 148.
42. Valente, J. S.; Cantu, M. S.; Cortez, J. G. H.; Montiel, R.; Bokhimi, X.; Salinas, E. L.; *J. Phys. Chem. C* **2007**, *111*, 642.
43. Pudi, S. M.; Mondal, T.; Biswas, P.; Biswas, S.; Sinha, S.; *Int. J. Chem. React. Eng.* **2014**, *12*, 151.
44. Lee, J.; Lee, E.; Joo, O.; Jung, K.; *Appl. Catal., A* **2004**, *269*, 1.
45. Rogatis, L. D.; Montini, T.; Lorenzut, B.; Fornasiero, P.; *Energy Environ. Sci.* **2008**, *1*, 501.
46. Zhang, R.; Kaliaguine, S.; *Appl. Catal., B* **2008**, *78*, 275.
47. Dumas, J. M.; Geron, C.; Kribii, A.; Barbier, J.; *Appl. Catal.* **1989**, *47*, L9.
48. Kang, M.; Song, M. W.; Kim, T. W.; Kim, K. L.; *Can. J. Chem. Eng.* **2002**, *80*, 63.
49. Jiang, Z.; Hao, Z.; Yu, J.; Hou, H.; Hu, C.; Su, J.; *Catal. Lett.* **2005**, *99*, 157.
50. Bridier, B.; Lopez, N.; Perez-Ramirez, J.; *J. Catal.* **2010**, *269*, 80.
51. Biswas, P.; Kunzru, D.; *Int. J. Hydrogen Energy* **2007**, *32*, 969.
52. Heracleous, E.; Lee, A. F.; Wilson, K.; Lemonidou, A. A.; *J. Catal.* **2005**, *231*, 159.
53. Riaz, N.; Chong, F. K.; Dutta, B. K.; Man, Z. B.; Khan, M. S.; Nurlaela, E.; *Chem. Eng. J.* **2012**, *185-186*, 108.

54. Yu, W.; Xu, J.; Ma, H.; Chen, C.; Zhao, J.; Miao, H.; Song, Q.; *Catal. Commun.* **2010**, *11*, 493.
55. Dumitriu, E.; Hulea, V.; *J. Catal.* **2003**, *218*, 249.
56. Khandan, N.; Kazemeini, M.; Aghaziarati, M.; *Appl. Catal., A* **2008**, *349*, 6.
57. Suelves, I.; Lazaro, M. J.; Moliner, R.; Echegoyen, Y.; Palacios, J. M.; *Catal. Today* **2006**, *116*, 271.
58. Rodrigues, R.; Isoda, N.; Gonçalves, M.; Figueiredo, F. C. A.; Mandelli, D.; Carvalho, W. A.; *Chem. Eng. J.* **2012**, *198-199*, 457.
59. Alhanash, A.; Kozhevnikova, E. F.; Kozhevnikov, I. V.; *Catal. Lett.* **2008**, *120*, 307.
60. Salazar, J. B.; Falcone, D. D.; Pham, H. N.; Datye, A. K.; Passos, F. B.; Davis, R. J.; *Appl. Catal., A* **2014**, *482*, 137.
61. Rode, C. V.; Mane, R. B.; Potdar, A. S.; Patil, P. B.; Niphadkar, P. S.; Joshi, P. N.; *Catal. Today* **2012**, *190*, 31.
62. Yadav, G. D.; Chandan, P. A.; Devendra, P. T.; *Ind. Eng. Chem. Res.* **2012**, *51*, 1549.
63. Hamzah, N.; Nordin, N. M.; Nadzri, A. H. A.; Nik, Y. A.; Kassim, M. B.; Yarmo, M. A.; *Appl. Catal., A* **2012**, *419*, 133.
64. Xia, S.; Zheng, L.; Nie, R.; Chen, P.; Lou, H.; Hou, Z.; *Chin. J. Catal.* **2013**, *34*, 986.
65. Montassier, C.; Dumas, J. M.; Granger, P.; Barbier, J.; *Appl. Catal., A* **1995**, *121*, 231.
66. Xia, S.; Du, W.; Zheng, L.; Chen, P.; Hou, Z.; *Catal. Sci. Technol.* **2014**, *4*, 912.

Submitted: November 28, 2014
Published online: May 15, 2015